Nanoscale

PAPER

View Article Online
View Journal | View Issue

Cite this: *Nanoscale*, 2024, **16**, 13445

Orchestration of ferro- and anti-ferromagnetic ordering in gold nanoclusters†

Nisha Mehla, Aritra Mukhopadhyaya, Shahjad Ali and Md. Ehesan Ali *

Received 28th February 2024,
Accepted 7th June 2024

DOI: 10.1039/d4nr00856a

rsc.li/nanoscale

The unpaired electron in the gold clusters (Au_n, n = no. of Au atoms) with an odd number of total electrons is solely responsible for the magnetic properties in the small-sized Au nano-clusters. However, no such unpaired electron is available due to pairing in the even number of atom gold clusters and behaving as a diamagnetic entity similar to bulk gold. In this work, we unveiled the spin-density distribution of odd Au_n clusters with n = 1 to 19 that reveals that a single unpaired electron gets distributed non-uniformly among all Au-atoms depending on the cluster size and morphology. The delocalization of the unpaired electron leads to the spin dilution approaching a value of ~1/n spin moments on each atom for the higher clusters. Interestingly, small odd-numbered gold clusters possess spin-magnetic moments similar to the delocalized spin moments as of organic radicals. Can cooperative magnetic properties be obtained by coupling these individual magnetic gold nanoparticles? In this work, by applying state-of-the-art computational methodologies, we have demonstrated ferromagnetic or anti-ferromagnetic couplings between such magnetic nanoclusters upon designing suitable organic spacers. These findings will open up a new avenue of nanoscale magnetic materials combining organic spacers and odd-electron nano-clusters.

1 Introduction

Ferromagnetically ordered spin systems are of great interest due to their potential applications in the field of spintronics.[1–6] Such systems could be used to generate a fully spin-polarized current. Various transition metal complexes and organic magnetic materials (OMMs) have been reported in this regard.[7–14]

Bulk gold is diamagnetic,[15] but the nanoworld unfolds a contrasting scenario with the experimentally observed magnetism in nanoparticles of gold.[16–25] The earliest mention of it came from the research conducted by Hori *et al.* in 1999 in which they focused on magnetization measurements involving gold nanoparticles (NPs) of 2.5 nm.[26] Yamamoto *et al.* provided the initial concrete experimental confirmation of ferromagnetic spin polarization by employing the X-ray magnetic circular dichroism (XMCD) technique on gold NPs shielded with polyallyl amine hydrochloride.[27]

The NPs composed of Au, Ag, and Cu have been observed to exhibit permanent magnetism at room temperature using XMCD and ^{197}Au Mössbauer spectroscopy.[28] Krishna *et al.* have observed ferromagnetic behaviour in $Au_{55}(PPh_3)_{12}Cl_6$ at room temperature.[29] At low temperatures, feeble ferromagnetic interactions have been detected in $Au_{25}(SCH_2CH_2Ph)^0$ using EPR and hysteresis experiments,[30,31] but were not observed using the SQUID magnetometer technique.[29]

Since the unearthing of magnetism in nano gold, plenty of theories have been crafted to explain this phenomenon. Zhang *et al.* investigated the electronic behavior of Au NPs (~2 nm) capped with dendrimer and thiol molecules which reveals that d-electron distribution in the Au NPs can be tuned by selective capping.[32,33] When Au NPs are capped with strongly interacting thiols, the number of holes in the 5d band increases.[34,35] The ferromagnetism in gold has also been associated with 5d localized holes generated through the Au–S bond.[36] It has been shown that thiolate induced magnetism occurs in gold.[37] It has been reported that the large orbital component of 5d electrons is the origin of spontaneous spin polarization in gold NPs.[25,38] The gold NPs display ferromagnetic spin polarization which is found to be dependent on the size of NPs.[16,39–41] In 2021, Li *et al.* used the electron paramagnetic resonance (EPR) technique to explore magnetism in Au_{25} and Au_{133} clusters.[31] Their findings indicate that in Au NCs, magnetism isn't chiefly linked to size or ligands, but rather to the electron count.

In the experimental study by Hasan *et al.*,[42] which provides the first experimental evidence for the adsorption of intact

Institute of Nano Science and Technology, Sector-81, Mohali, Punjab 140306, India. E-mail: ehesan.ali@inst.ac.in

†Electronic supplementary information (ESI) available: Energetics of isolated Au_n clusters, molecular orbital plots of odd and even clusters, single point energies and the magnetic exchange coupling constant (2J) for coupled clusters using the Yamaguchi and Noodleman formula, Löwdin spin population distribution in isolated Au_n clusters and when clusters are coupled *via* a benzene spacer, the effect of the capping agent SH_2 on the spin magnetic moment of Au atoms, and variation of the overlap integral with magnetic exchange coupling. See DOI: https://doi.org/10.1039/d4nr00856a

thiols on the gold clusters analysed by ^{1}H NMR spectroscopy, it was found that when thiol coverage is lower (less than 2 molar equiv. of thiol), removal of hydrogen is favoured. Thus, the experimental conditions influence which of the two competing mechanisms, dissociative or undissociative, will occur. Another experimental work has also concluded that the –SH bond does not cleave during CH_3SH adsorption on the Au(111) surface under ultra-high vacuum (UHV) conditions.[43] It has been found that CH_3SH and C_3H_7SH adsorb on the Au(111) surface without -SH bond scission but the -SH bond dissociates on the defective Au surface.[44] One of the theoretical studies suggests that thiolates and "intact" SH species can exist together.[45] It has been suggested that long alkyl chain thiols adsorb by physisorption, while thiols with a short alkyl chain adsorb by chemisorption.[46] A recent study by Inkpen *et al.*[47] demonstrates that gold–sulfur interfacial coupling in the self-assembled monolayers of dithiols is through the physisorbed interaction and thiol hydrogen is retained.

However, to comment upon which gold–thiol binding process is more favourable is out of the scope of this work and based upon the results of the above-mentioned experimental and theoretical studies we have chosen one of the possibilities of gold–thiol binding ((RS–H) remains intact,[42–47] homolytic cleavage (–RS$\dot{}$)[48,49] and the heterolytic cleavage ($-RS^-$)[50]) with thiol as the "intact" species to show how the gold nanoclusters can couple (FM/AFM) *via* the coupler.

Despite the knowledge of the magnetic behaviour of the gold nanoclusters, a comprehensive understanding is lacking about the delocalization of the unpaired electron *i.e.* the source of magnetic properties among the constituent Au-atoms. Our study aims to understand the magnetic behaviors of small gold nanoclusters. The unambiguous identification of the magnetic gold nano-clusters encourages us to ask the natural question: can magnetic ordering be induced among these tiny nano-magnets? Here we have investigated a strategy of coupling odd Au_n clusters with n = 3 to 19 designing an organic spacer that sheds light on harnessing the cooperative magnetic ordering utilising gold nanoclusters.

The magnetic ordering in the gold nanoclusters using organic spacers is crucial from the device application perspective in the field of spintronics, quantum computing and various technological applications like high density memory storage, magnetic devices, nanocatalysis and biomedicine.

2 Theoretical model and computational methodology

2.1 Theoretical model

The magnetic exchange interaction between two spin centers 1 and 2 is usually expressed by the Heisenberg–Dirac–Van Vleck spin Hamiltonian,

$$\hat{H}_{\mathrm{HDVV}} = -2J\hat{S}_1 \cdot \hat{S}_2 \quad (1)$$

where $2J$ is the magnetic exchange coupling constant which is the measure of the magnetic interaction strength between the spin centers, and $\hat{S}_1$ and $\hat{S}_2$ are the respective spin angular momentum operators. A positive $2J$ value indicates a preference for ferromagnetic coupling, where the spin centers align in parallel, promoting a high spin state. Conversely, a negative $2J$ value suggests a propensity for antiferromagnetic coupling, wherein the spin centers align anti-parallel, favoring a low spin state. One of the initial approaches for estimating magnetic exchange coupling was suggested by Noodleman.[51,52] This method involves employing broken symmetry solutions for low-spin states. Noodleman's formula for evaluation of the magnetic exchange coupling constant ($2J$ value) is

$$2J = -\frac{2(E_{\mathrm{HS}} - E_{\mathrm{BS}})}{{s_{\max}}^2} \quad (2)$$

where E_{BS} is the energy of low spin solution, E_{HS} is the high spin energy, and $s_{\max}$ is the total spin of high spin state. The broken symmetry state is an equal mixture of the lowest and highest spin states. A more general approach toward the computation of the $2J$ value was given by Yamaguchi *et al.*[53] as given below,

$$2J = -\frac{2(E_{\mathrm{HS}} - E_{\mathrm{BS}})}{\langle S^2\rangle_{\mathrm{HS}} - \langle S^2\rangle_{\mathrm{BS}}} \quad (3)$$

In our analysis, we've employed the formula (3) established by Yamaguchi *et al.* We have noticed that $s_{\max}$ = 1 and the difference ($\langle S^2\rangle_{\mathrm{HS}} - \langle S^2\rangle_{\mathrm{BS}}$) is nearly equal to 1.0 for all the systems. In the weak orbital overlap regions, the Yamaguchi formula (eqn (3)) can be reduced to the Noodleman formula (eqn (2)). Since the systems involved in our investigation have weak overlap between the magnetic orbitals, the $2J$ values (refer to the ESI†) obtained using eqn (2) and (3) are almost equal.

2.2 Computational methodology

The optimization of Au_n clusters with n ranging from 1 to 20 and odd Au_n clusters coupled *via* a π-conjugated molecule, thiol functionalized diethynylbenzene (t-DEB), was performed using the B3LYP hybrid functional[54] and def2-TZVP[55] basis set. The preference for the B3LYP functional stems from its established efficacy in accurately determining the exchange coupling constants.[56–61] The gold clusters were treated using the spin-unrestricted Kohn Sham (UKS) method within the DFT framework. The RI approximation in conjunction with the auxiliary basis set def2/J was employed. In order to differentiate between the J used in the auxiliary basis set def2/J and the magnetic exchange coupling constant $2J$, we have used italicized J in $2J$ and non-italicized J in def2/J. For the Hartree–Fock exchange calculations, a Chain of Spheres (COSX) numerical integration method was utilized to enhance the speed while preserving accuracy.[62] We explored the electronic configurations of odd clusters, encompassing both doublet and quartet states, and examined even clusters, considering singlet and triplet states. The odd clusters predominantly assume a doublet ground state, while even clusters exhibit a singlet ground state. For clusters connected through the

spacer, *meta* t-DEB, the geometry has been optimized in the triplet state, whereas when connected *via para* t-DEB, the geometry optimization has been conducted in the broken symmetry (BS) state which is their respective ground state.

To facilitate magnetic exchange coupling analysis, we performed single-point calculations utilizing the BS-DFT method in the ORCA quantum chemical code.

3 Results and discussion

Unpaired spin-bearing odd Au_n clusters can be considered atomic scale nanomagnets. The spin density distribution of the DFT-optimized geometries of the Au_n (n = 1,2...20) clusters has been discussed in the following subsection. Upon designing an organic spacer, capable of effectively coupling the stable organic radicals, the magnetic ordering of the Au_n clusters has been studied. The predicted ordering of magnetic ordering has been rationalized from the electronic structure.

3.1 Au_n clusters: geometries and spin distribution

The gold nanoclusters' geometries used in the present work represent the global minimum geometries. We have used the global minimum geometries reported by Khatun *et al.*[63] as the initial geometries. The authors obtained these geometries by generating several trial geometries and performing a gradient based local optimization of these trial geometries. In this work, we have further optimized these geometries at the B3LYP/def2-TZVP level. We have optimized the Au_n, n = 1 to 20 clusters in the different spin states.[63–66] It is observed that odd and even gold clusters have the doublet and singlet ground states, respectively (shown in section S1 of the ESI†). The optimized geometries of Au_n clusters are shown in Fig. 1.

It is observed that Au_2 to Au_{10} clusters favor planar geometries[67] and beyond Au_{10}, gold clusters show a shift from 2D to 3D configurations. This is in agreement with the previously reported 2D to 3D transition of gold clusters.[63–66,68,69]

These structural variations in the gold clusters are due to the different nature of hybridization in frontier molecular orbitals. The singly occupied molecular orbital (SOMO) of the single Au atom is completely of s character which is quite obvious from the electronic configuration of the gold atom, with one unpaired electron in the 6s shell. Each cluster is formed by adding one more atom to the preceding cluster. The addition of one more gold atom in the vicinity of a single Au atom forms an Au–Au bond due to the overlapping of the s–s

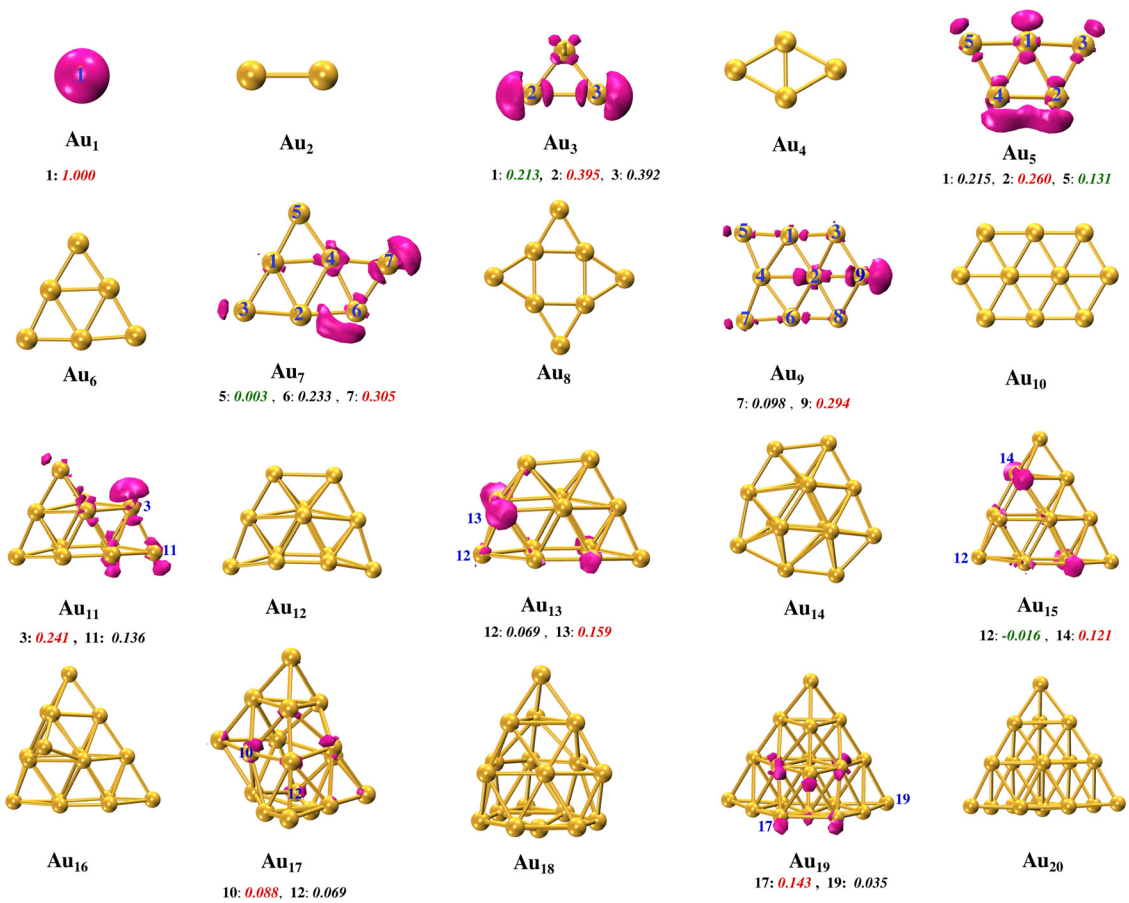

Fig. 1 The spin density of the optimized geometries of Au_n, n = 1 to 20 clusters at the B3LYP/def2-TZVP level. The numbers shown below show the spin population distribution over the specific atoms (red color for the highest spin population and green for the lowest spin population.).

orbitals. The Au_2 cluster has a Au–Au bond length of 2.53 Å, closely mirroring the experimentally observed bond length of around 2.49 Å.[70] With the inclusion of a third atom to the Au_2 cluster, bonding between the atoms of the Au_3 cluster is no longer due to the s orbitals only but the role of hybridization of s, p, and d orbitals comes into play (see Fig. S1 and S2, ESI†). It is quite natural to assume that Au_3 would have an equilateral triangle geometry but after optimization, it shows an isosceles triangular structure, characterized by two equal bond lengths of 2.66 Å and a longer length of 3.26 Å which is attributed to the antibonding s–s orbitals. The Au_4 cluster is rhombus-shaped with uniform side lengths of 2.77 Å. The Au_5 cluster exhibits a distinctive W shape, showcasing the bi-capped triangle geometry. The Au_6 cluster assumes a planar triangular arrangement, featuring an outer equilateral triangle with dimensions measuring 5.7 Å and an inner, smaller equilateral triangle measuring 2.9 Å on each side. The Au_7 cluster displays a capped triangle geometry, and Au_8 and Au_9 clusters embrace a tetra-crowned rhombus and bi-capped hexagon geometries respectively. Au_{19} is characterized by a truncated tetrahedral shape. The Au_{20} cluster shows a perfect tetrahedral geometry.

Since the even gold clusters have a singlet ground state, they do not have a spin magnetic moment, as all the electrons are paired. Unlike the even clusters, odd gold clusters always have a doublet ground state irrespective of the size of the cluster. This is due to the odd number of total electrons in the odd gold clusters which always leave one electron aloof, giving rise to the total magnetic moment of $1\mu_B$ on the odd gold clusters.[37] These observations are in alignment with the study performed by Zhu *et al.* on the magnetic properties of gold clusters.[67] The spin population distribution over the atoms of odd gold clusters is shown in Fig. 2. It reveals that the spin magnetic moment is non-uniformly distributed on the different atoms of gold clusters. For example, in Au_3, $0.79\mu_B$ of the spin magnetic moment is distributed over two of its constituent atoms, while the remaining $0.21\mu_B$ resides on the third atom. Similarly, in Au_9, $0.29\mu_B$ of the magnetic moment resides on one atom (marked as atoms 9 in Fig. 1), while the remaining $0.71\mu_B$ is distributed among the other eight atoms.

The more fascinating fact pertains to the constant spin magnetic moment of $1\mu_B$ over the odd Au_n clusters, irrespective of their cluster size. But as the cluster size progresses, the spin gets diluted as $1/n\ \mu_B$ per atom assuming the uniform distribution of the spin magnetic moment on the atoms of the gold cluster. However, it is obvious that smaller clusters have a higher average magnetic moment per atom than larger clusters. However, the smaller clusters display a larger deviation of the spin magnetic moment per atom from the average distribution curve ($1/n\ \mu_B$ per atom) in comparison to the higher-order clusters (shown in Fig. 2). Thus, the small odd gold clusters show a non-uniform distribution of the spin magnetic moment on the atoms of gold clusters which becomes uniform for the larger gold clusters.

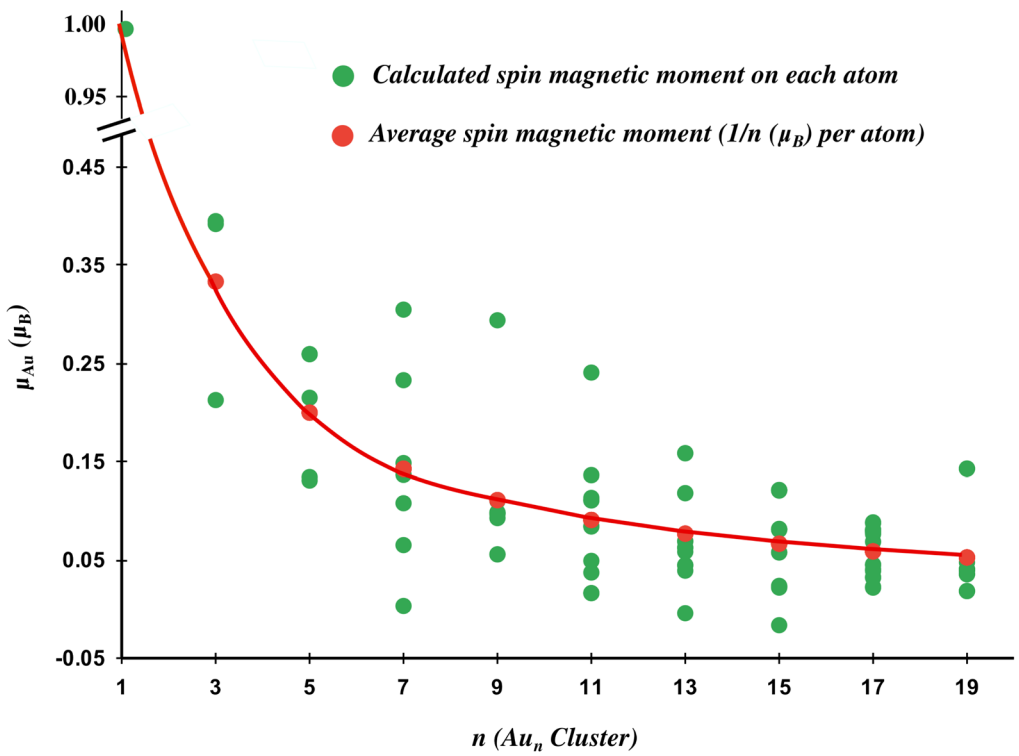

Fig. 2 The Löwdin spin population distribution over the atoms of Au_3 to Au_{19} clusters, represented by green-coloured data points. Red-colored data points depict the hypothetical case of average spin population distribution ($1/n\ \mu_B$ per atom).

3.2 Ordering of magnetic moment in gold clusters

One of the key strategies to harness the magnetic ordering of the spin-bearing organic as well as inorganic moieties is to use a conjugated molecular framework as a coupler through which the magnetic exchange can be communicated between two spatially separated spin sources.[9–13,71–76] The π electron-rich aromatic organic molecules, such as benzene, are an excellent choice in this context. To exhibit an efficient ordering of magnetic moments, the coupled gold clusters must retain their magnetic properties when they are connected *via* an organic spacer. The spatial separation of the connected Au_n cluster must be sufficient to inhibit the clusters from collapsing into a single cluster. Keeping this fact in mind, diethynylbenzene (DEB) was used as the organic spacer as shown in Fig. 3. Furthermore, to connect the gold clusters and organic spacer we have functionalized the spacer with the thiol group, which is abbreviated as t-DEB. Nitronyl nitroxide (NN) and Blatter's radical (Bl) are two popular radicals that have been observed to show definite magnetic ordering when coupled *via* organic spacers.[9,11,13,77] To test the effectiveness of the DEB molecule as a coupler, both the *meta* (*m*) and *para* (*p*) DEB have been used to couple the spin centers of the aforementioned organic radicals (Fig. 3). The nitronyl nitroxide and Blatter's radical coupled with *m*-DEB show a FM exchange interaction of 7.44 cm^{-1} and 3.60 cm^{-1}, respectively, while an AFM exchange interaction of −225.3 cm^{-1} and −16.22 cm^{-1} is observed with the *p*-DEB coupler (Table 1). This is in agreement with the previously reported nature of coupling (FM/AFM) of *meta*/*para*-connected organic radicals through the benzene coupler.[9,71,78] This suggests that the DEB organic spacer can effectively couple the organic radicals.

When the single Au atom (Au_1) is coupled *via* the *m*-tDEB (*p*-tDEB) coupler as shown in Fig. 3, a very strong ferromagnetic (antiferromagnetic) coupling with 2*J* values as high as 27.88 (−196) cm^{-1} is observed (Table 1). Henceforth, the coupling of Au_n clusters through the *meta* and *para* t-DEB couplers will be designated as Au_n-*m*-Au_n and Au_n-*p*-Au_n respectively. As discussed in the previous section, the distribution of the spin moments amongst the Au atoms is not the same for the isolated clusters. Consequently, the strength of the exchange interaction is also dependent on the atomic site to which the coupler is linked. In the ESI (section S4†), we have calculated the 2*J* values of the Au_n clusters, linked to the coupler *via* different atomic sites. Out of all possible combinations, the connection showing the highest 2*J* is further considered for understanding the variation of the strength of the magnetic coupling for the odd Au_n clusters which has been shown in Fig. 6. For the *meta*-coupled clusters, ferromagnetic ordering is observed for Au_9-*m*-Au_9 with the 2*J* value of 1.82 cm^{-1} using the B3LYP functional (Table 1). In contrast to the clusters connected through *para* t-DEB, Au_9-*p*-Au_9 exhibits antiferromagnetic coupling, underscored by the 2*J* value of 42.26 cm^{-1}. Thus, this is a clear indication that the magnetic moments arising out of the odd Au_n clusters could be ordered by interconnecting them through an organic spacer to get the FM/AFM coupling. Table 1 indicates stronger antiferro-

Table 1 Single point energies and calculated magnetic exchange coupling constants (2*J*) for different spin sources with the *m*/*p*-DEB coupler designated as *m*′/*p*′ for nitronyl nitroxide (NN) and Blatter's radical (Bl) and the *m*/*p*-tDEB coupler represented as *m*/*p* for the Au atom

	Energy (E_h)		$\langle S^2 \rangle$		
	BS	HS	BS	HS	2*J* (cm^{-1})
NN-*m*′-NN	−1450.665005	−1450.665022	1.14	2.14	7.44
NN-*p*′-NN	−1450.669604	−1450.669105	1.17	2.14	−225.30
Bl-*m*′-Bl	−2174.975354	−2174.977133	1.03	2.03	3.60
Bl-*p*′-Bl	−2174.977170	−2174.977133	1.03	2.03	−16.22
Au_1-*m*-Au_1	−1452.165381	−1452.165445	1.00	2.01	27.88
Au_1-*p*-Au_1	−1452.167157	−1452.166706	0.99	2.00	−196.34
Au_9-*m*-Au_9	−3624.244986	−3624.244990	1.01	2.01	1.82
Au_9-*p*-Au_9	−3624.245767	−3624.245670	1.01	2.01	−42.26

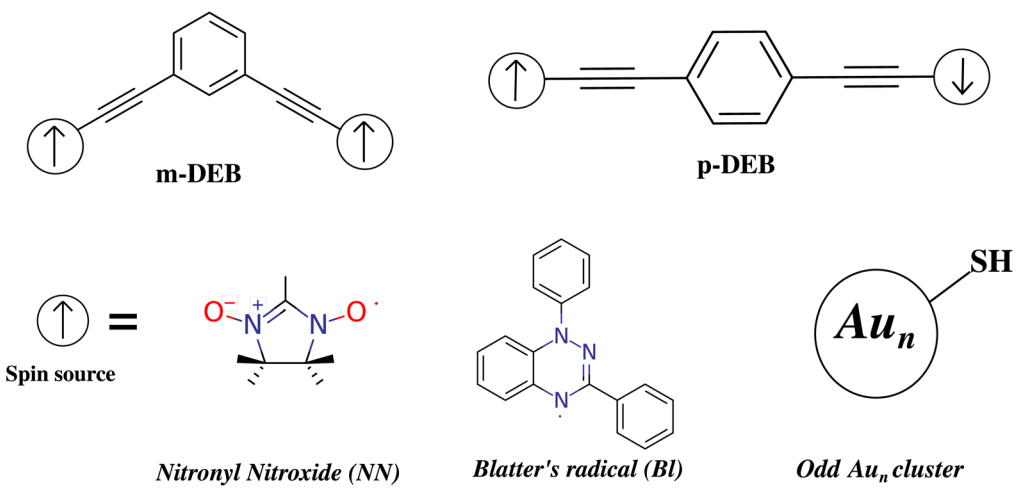

Fig. 3 The schematics of (*meta*/*para*) diethynylbenzene (*m*-DEB/*p*-DEB) and the thiol functionalized *m*/*p*-tDEB couplers. The circle with spin up and down arrows represents different spin sources: nitronyl nitroxide (NN), Blatter's radical (Bl), and the odd gold clusters.

magnetic exchange interactions than ferromagnetic interactions[71,78] (refer to subsection S4.1 of the ESI†).

In order to verify the dependence of $2J$ on the functional, we have calculated $2J$ values for Au_1-*m*/*p*-Au_1 and Au_9-*m*/*p*-Au_9 using different functionals, namely local and gradient corrected functionals (BLYP, PBE), hybrid functionals (B3LYP, PBE0), *meta* GGA functional (TPSS), and hybrid *meta* GGA functional (TPSSh, M06). Local and gradient corrected functionals overestimate the $2J$ (refer to section S3.1 of the ESI† for variation of $\langle S^2 \rangle_{BS}$ value for different functionals), but the nature of magnetic coupling through the *meta* and *para* organic spacer using every functional is found to be the same *i.e.*, FM and AFM respectively (Fig. 4).

For the purpose of benchmarking, we have also done the CASSCF and CASSCF-NEVPT2 calculations whose results are provided in section 2 of the ESI† for the proto typical case of Au_1-*m*/*p*-Au_1. Here, our objective is only to verify the nature of coupling through the *meta* and *para* couplers. The $2J$ values obtained with CASSCF(6,6) and CASSCF-NEVPT2(6,6) for Au_1-*m*-Au_1 are 2.86 cm^{-1} and 7.28 cm^{-1} respectively, while for Au_1-*p*-Au_1, $2J$ values are −9.77 cm^{-1} and −36.93 cm^{-1}. Once again, the multireference calculations for the prototypical Au_1 case confirm the FM and AFM ordering with *meta* and *para* spacers respectively.

The anchoring thiol groups play a crucial role in forming the exchange pathways between the coupled Au_n clusters. As shown in Fig. 5, the sulfur atoms of the –SH groups retain a

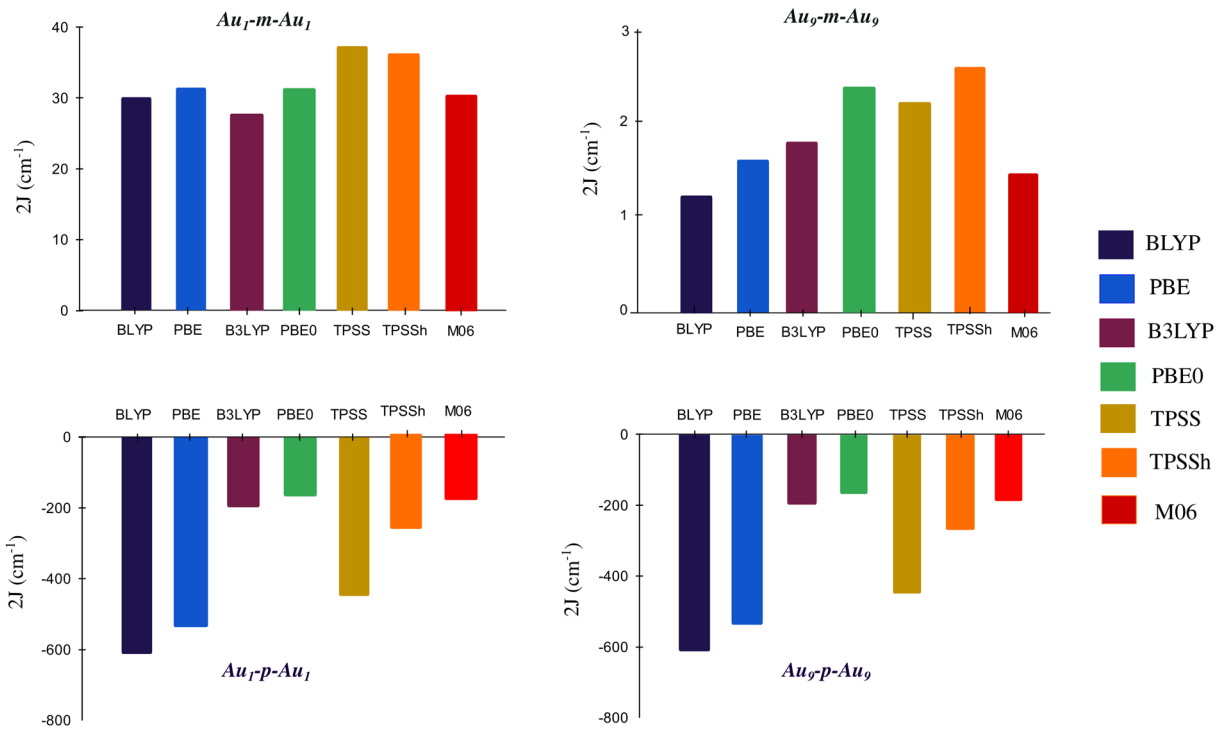

Fig. 4 Variation in $2J$ with different functionals for Au_1-*m*/*p*-Au_1 and Au_9-*m*/*p*-Au_9 with def2-TZVP as the basis set.

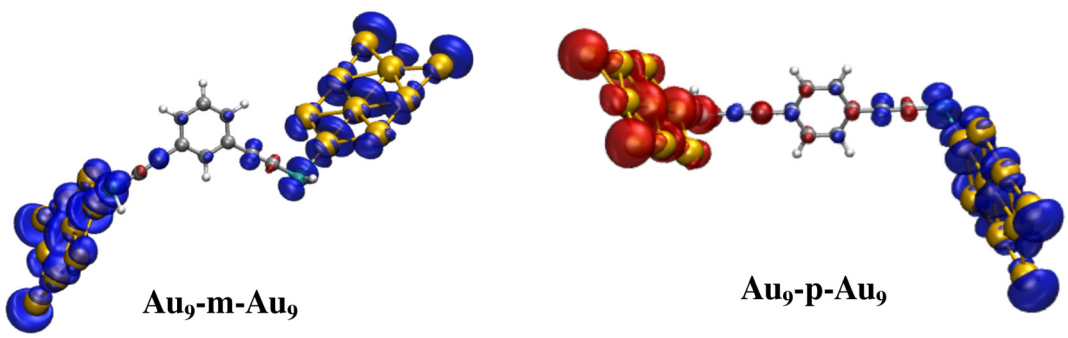

Fig. 5 Spin density plots for the optimized geometries of Au_9-*m*/*p*-Au_9 at the UB3LYP /def2-TZVP/def2/J level. The α and β spins are shown in blue and red color respectively with the isosurface value 0.001 μ_B $Å^{-3}$.

significant amount of the spin density from the Au_9 clusters and take part in the π conjugation with the t-DEB spacer. The ferromagnetic coupling for the *meta* connection and the antiferromagnetic coupling for the *para* connection can be rationalized by applying the simple spin alternation rule of the aromatic couplers. In the case of *meta* t-DEB, the spin sources from the two Au clusters are connected *via* $2N + 1$ number of atoms, where N is the number of conjugated π-bonds and hence gives ferromagnetic coupling, whereas, in the case of *para* t-DEB, there are 2N atoms present in the exchange pathways between the Au_n clusters which results in the antiferromagnetic ordering of the nanomagnets. However, the spin polarization of the sulfur atom is not the same for all the clusters considered here. It has been observed that higher spin polarization of organic spacers induced by the Au_n cluster results in a larger magnetic exchange interaction.

When we move from a single Au atom to odd Au_n clusters, the nature of magnetic ordering remains the same. However, we witnessed a substantial decrement in the magnetic coupling strength for both kinds of exchange pathways. The exchange interactions for the gold clusters using the *meta* coupler (*m*-tDEB) are shown in Fig. 6. The $2J$ values obtained for the coupled odd gold clusters are in the range of 0.02 to 2.32 cm^{-1}, with the lowest and the highest $2J$ corresponding to Au_3-*m*-Au_3 and Au_7-*m*-Au_7, respectively. For the antiferromagnetic ordering of the magnetic moments, which has been observed using *para* t-DEB as a coupler (Fig. 6), the highest $2J$ equal to −42.26 cm^{-1} has been obtained for Au_9-*p*-Au_9. With Au_{11}-*p*-Au_{11}, Au_7-*p*-Au_7 and Au_5-*p*-Au_5, −30.9 cm^{-1}, −25.6 cm^{-1}, and −20.3 cm^{-1} respectively have been obtained as the $2J$ values, showcasing stronger antiferromagnetic coupling in these cases. Magnetic exchange interactions can also be observed when –SH is replaced with S^- (anion) and $\dot{S}$ (radical). But in the case of the $\dot{S}$ radical, its free electron quenches the magnetic moment arising from odd Au_n clusters, but the interesting aspect is that exchange interactions can now be observed with even Au_n clusters (refer to subsection S4.2 of the ESI† for $2J$ values in different S–Au linkages).

In the case of Au_3-*m*/*p*-Au_3 and Au_{13}-*m*/*p*-Au_{13} to Au_{19}-*m*/*p*-Au_{19} clusters, we have observed a significant reduction in magnetic interaction strength between the magnetic centers. While it's expected that the magnetic interaction strength decreases as the cluster size increases, it's notable that with just one unpaired electron present, there is a diminished spin distribution across the atoms of the Au_n cluster known as the spin dilution effect. However, the case of Au_3-*m*/*p*-Au_3 is particularly interesting. Here, the magnetic interaction strength is unexpectedly low, despite the presence of only three atoms and the unpaired spin being distributed among them. Following this observation, we further investigated the spin population distribution in the isolated Au_3 cluster and in the case where clusters are connected through benzene (refer to section S5 of the ESI† for spin density distribution). The atom of Au_3 cluster attached to the SH group, whether it is 1, 2, or 3; regardless of the spin density in the isolated case that atom's spin magnetic moment reduces to $0.13\mu_B$ and the spin moment redistribution leads to spin delocalization over the other two atoms of the cluster, with most of the spin moment ($0.986\mu_B$) still lying with the Au_3 cluster which suggests that the spin centers exhibit a propensity to avoid coupling pathways through the organic spacer. Also, it is interesting to note here the change in the geometry of the Au_3 cluster from an isosceles triangle to the equilateral triangular shape when connected through the coupler.

3.3 Factors influencing exchange coupling magnitude

3.3.1 Impact of gold cluster's coupling site. The magnitude of exchange interactions is also found to be dependent upon the atom of the gold cluster utilized to make connection with the thiol group. This dependence is attributed to the non-

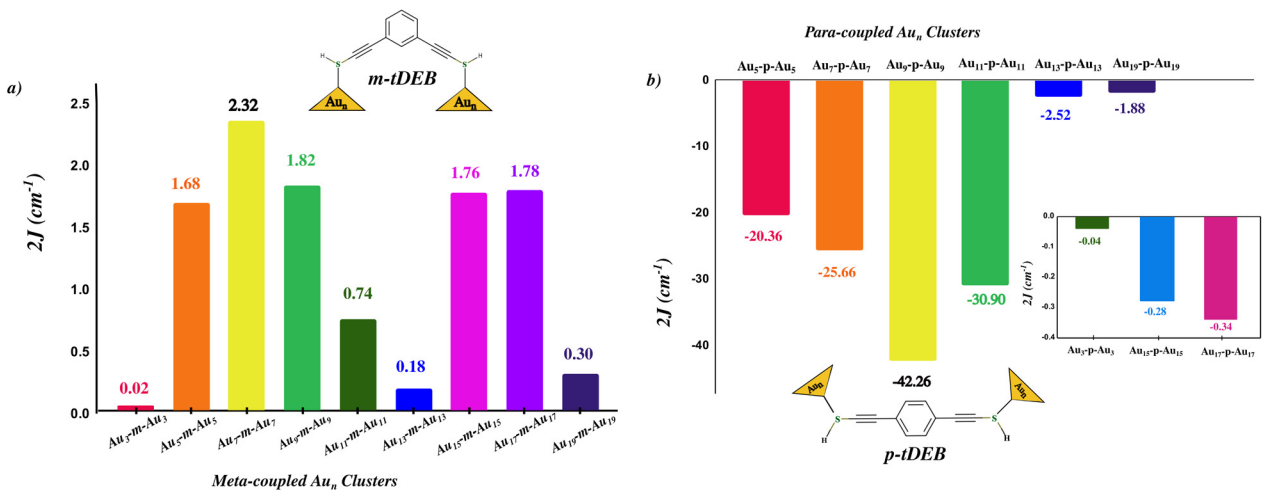

Fig. 6 (a, b) Magnetic exchange coupling constant variation in odd Au_n clusters, n = 3,...,19 coupled through the t-DEB (*meta* and *para*) organic spacer represented as Au_n-*m*-Au_n and Au_n-*p*-Au_n. The inset of (b) shows the $2J$ values for Au_3-*p*-Au_3, Au_{15}-*p*-Au_{15} and Au_{17}-*p*-Au_{17} as they have lower values in comparison to the other Au_n-*p*-Au_n geometries. Refer the ESI† for *para* and *meta* coupled Au_n clusters.

Table 2 Single point energies and calculated magnetic exchange coupling constants ($2J$) for Au_1-*m*/*p*-Au_1 and Au_9-*m*/*p*-Au_9 clusters with and without the capping agent (SH_2)

	Energy (E_h)		$\langle S^2 \rangle$		
	BS	HS	BS	HS	$2J$ (cm^{-1})
Au_1-*m*-Au_1	−1452.165381	−1450.165445	1.01	2.01	27.88
Au_1-*m*-Au_1 (SH_2)	−2250.885193	−2250.885235	1.01	2.01	18.48
Au_1-*p*-Au_1	−1452.167157	−1452.166706	0.99	2.00	−196.34
Au_1-*p*-Au_1 (SH_2)	−2250.887052	−2250.886478	0.99	2.00	−248.04
Au_9-*m*-Au_9	−3624.244986	−3624.244990	1.01	2.01	1.82
Au_9-*m*-Au_9 (SH_2)	−5221.742238	−5221.742254	1.01	2.01	6.90
Au_9-*p*-Au_9	−3624.245767	−3624.245670	1.01	2.01	−42.26
Au_9-*p*-Au_9 (SH_2)	−5221.741919	−5221.741769	1.00	2.00	−65.02

uniform spin population distribution over the cluster's atom. Whenever we involve an atom with a higher spin density in the case of an isolated cluster to attach it with the SH group, higher magnetic interaction strength between the spin centers is observed because of the strong delocalization of the spin magnetic moment throughout the coupling pathway with the maximum of it retained with sulphur of the thiol group, which is manifested in the higher $2J$-values (refer to section S4 of ESI†); *e.g.*, atom no. 1, 2 in the Au_5 cluster, atom 6, 7 in Au_7, atom 9 in Au_9, atom 3 in Au_{11} and so on. On the other hand, the utilization of atoms with a lower spin density gives minimal magnetic exchange interaction between the odd Au_n clusters coupled *via* t-DEB; for example atom 5 in Au_5 and Au_7, atom 7 in Au_9, *etc*. As in this case, most of the spin magnetic moment remains with the gold cluster itself.

Magnetic exchange interactions also depend upon the shape of the magnetic orbitals, for instance the nature of orbitals in the case of AFM interactions is disjoint while FM interactions involve non-disjoint orbitals[79,80](refer to subsection S4.0.3 of the ESI†).

3.3.2 Effect of the capping agent (SH_2). The small odd Au_n clusters with n = 5, 7, 9 when coupled with an organic spacer display quite good FM/AFM ordering. There are several experimental shreds of evidence of synthesizing Au NPs.[29,81–84] But thiol-capped Au NPs are quite popular in the literature for stabilizing gold nanoclusters to utilize them in practical applications. To investigate, can the capping agent protect and keep the magnetic ordering of coupled Au NCs intact? In our endeavor to evaluate how the presence of the capping agent[83,84] SH_2 affects the coupling strength between odd gold clusters, which are linked together through the *m*-tDEB and *p*-tDEB coupler, we have bound one SH_2 group to the Au atom and two SH_2 groups to the edge atoms of the Au_9 cluster, allowing us to scrutinize how this agent shapes the coupling dynamics in Au_1-*m*/*p*-Au_1 and Au_9-*m*/*p*-Au_9 configurations.

Comparing the scenarios with and without the capping agent for Au_1 and Au_9 coupled through *m*/*p*-tDEB outlined in Table 2, it's evident that the incorporation of SH_2 capping effectively safeguards and enhances the inherent magnetism within the gold atom as well the Au_9 cluster. This is reflected in the elevated $2J$-values after binding the capping agent to the gold atom and edge atoms of the Au_9 cluster except in Au_1-*m*-Au_1 where the Au–S bond length is 3 Å, highest among all the cases. This enlargement of Au–S bond length moves the spin sources far away from the coupler, thereby reducing exchange interactions. Otherwise, except for Au_1-*m*-Au_1, in all the other cases spin density plots (see Fig. 7) suggest that attachment of the capping agent increases the spin magnetic moment

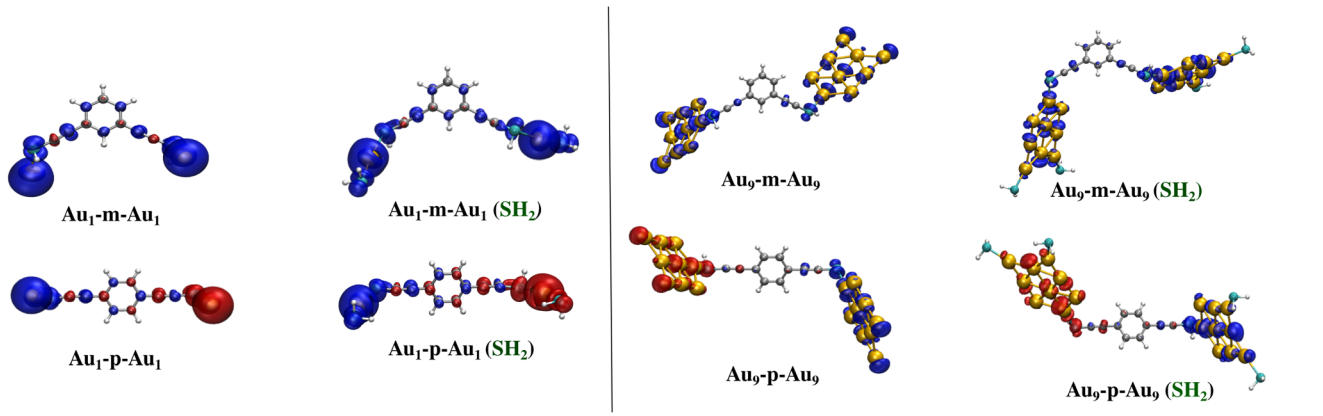

Fig. 7 Spin density of the optimized geometries of the Au atom and Au_9 clusters coupled *via* t-DEB, computed at the UB3LYP/def2-TZVP(ECP for Au)/def2/J level. The α and β spins are shown in blue and red color respectively with the isosurface value 0.001 μ_B $Å^{-3}$.

towards the coupler pathway, thereby increasing the exchange interactions.

4 Conclusion

In the odd Au_n (n = 1,3, ... 19) clusters, one unpaired electron, responsible for the magnetism in nano-clusters, becomes distributed amongst the constituent Au atoms in an unsymmetrical manner. As the cluster size expands, this unitary spin magnetic moment becomes progressively apportioned among the increasing number of constituent atoms, thereby converging towards an approximate $1/n\ \mu_B$ per atom. When two such one-electron paramagnetic Au-nanoclusters are coupled *via* an organic spacer, thiol-functionalized diethynylbenzene (t-DEB), definite magnetic ordering can be obtained. The *meta* and *para* t-DEB spacers result in the ferro and antiferromagnetic ordering of the magnetic moments. The π-conjugation in the organic spacers avail spin-altered exchange pathways to facilitate the ferro (antiferro) magnetic coupling in the *meta* (*para*)-connected Au-nanoclusters. The spin moments of the Au_n clusters make the linker thiol groups spin polarised, which in turn takes part in the conjugation with the coupler and facilitates the exchange mechanisms.

Author contributions

MEA conceptualized the project, supervised the work and secured funding. NM did computational data curation, data analysis and has written the initial draft. AM and SA contributed to the manuscript preparation and data analysis.

Conflicts of interest

There are no conflicts to declare.

Acknowledgements

Financial support from the Department of Science and Technology through SERB-CRG Project No. CRG/2022/008683 is gratefully acknowledged. S. A. thanks CSIR India for the SRF fellowship with Grant No. 09/1129(0027)/2020-EMR-I.

References

1 X. Li and J. Yang, First-principles design of spintronics materials, *Natl. Sci. Rev.*, 2016, **3**, 365–381.
2 C. Herrmann, G. C. Solomon and M. A. Ratner, Organic radicals as spin filters, *J. Am. Chem. Soc.*, 2010, **132**, 3682–3684.
3 W. Han, Y. Otani and S. Maekawa, Quantum materials for spin and charge conversion, *npj Quantum Mater.*, 2018, **3**, 27.
4 A. Hirohata, K. Yamada, Y. Nakatani, I.-L. Prejbeanu, B. Diény, P. Pirro and B. Hillebrands, Review on spintronics: Principles and device applications, *J. Magn. Magn. Mater.*, 2020, **509**, 166711.
5 A. Bajaj, P. Kaur, A. Sud, M. Berritta and M. E. Ali, Anomalous effect of quantum interference in organic spin filters, *J. Phys. Chem. C*, 2020, **124**, 24361–24371.
6 M. E. Ali, V. Staemmler, F. Illas and P. M. Oppeneer, Designing the redox-driven switching of ferro-to antiferromagnetic couplings in organic diradicals, *J. Chem. Theory Comput.*, 2013, **9**, 5216–5220.
7 T. R. Felthouse and D. N. Hendrickson, Magnetic exchange interactions in transition-metal dimers. 12. Structural and magnetic characterization of the di-. mu (1,3)-azido complex [Cu2(Me5dien)2(N3)2](BPh4)2 and similar di-.+-. (1,3)-azido copper(II) dimers. Unusual zero-field splitting in the electron paramagnetic resonance spectra, *Inorg. Chem.*, 1978, **17**, 444–456.
8 P. Gopal, R. De Gennaro, M. S. dos Santos Gusmao, R. A. R. Al Orabi, H. Wang, S. Curtarolo, M. Fornari and M. B. Nardelli, Improved electronic structure and magnetic exchange interactions in transition metal oxides, *J. Phys.: Condens. Matter*, 2017, **29**, 444003.
9 M. E. Ali and S. N. Datta, Broken-symmetry density functional theory investigation on bis-nitronyl nitroxide diradicals: influence of length and aromaticity of couplers, *J. Phys. Chem. A*, 2006, **110**, 2776–2784.
10 M. E. Ali, P. M. Oppeneer and S. N. Datta, Influence of Solute- Solvent Hydrogen Bonding on Intramolecular Magnetic Exchange Interaction in Aminoxyl Diradicals: A QM/MM Broken-Symmetry DFT Study, *J. Phys. Chem. B*, 2009, **113**, 5545–5548.
11 R. Khurana, A. Bajaj and M. E. Ali, How Plausible Is Getting Ferromagnetic Interactions by Coupling Blatter's Radical via Its Fused Benzene Ring?, *J. Phys. Chem. A*, 2020, **124**, 6707–6713.
12 R. Khurana, A. Bajaj and M. E. Ali, Tuning the magnetic properties of a diamagnetic di-Blatter's zwitterion to antiferro-and ferromagnetically coupled diradicals, *Phys. Chem. Chem. Phys.*, 2022, **24**, 2543–2553.
13 A. Bajaj and M. E. Ali, First-principle design of Blatter's diradicals with strong ferromagnetic exchange interactions, *J. Phys. Chem. C*, 2019, **123**, 15186–15194.
14 S. Shil, D. Bhattacharya, A. Misra and D. J. Klein, A high-spin organic diradical as a spin filter, *Phys. Chem. Chem. Phys.*, 2015, **17**, 23378–23383.
15 E. Vogt, in *Magnetism and Metallurgy*, ed. A. Berkowitz and E. Kneller, Academic Press, 1969, vol. 1, pp. 252.
16 R. Magyar, V. Mujica, M. Marquez and C. Gonzalez, Density-functional study of magnetism in bare Au nanoclusters: Evidence of permanent size-dependent spin polarization without geometry relaxation, *Phys. Rev. B: Condens. Matter Mater. Phys.*, 2007, **75**, 144421.
17 L. D. Marks, Experimental studies of small particle structures, *Rep. Prog. Phys.*, 1994, **57**, 603.

18 C. L. Cleveland, U. Landman, T. G. Schaaff, M. N. Shafigullin, P. W. Stephens and R. L. Whetten, Structural evolution of smaller gold nanocrystals: The truncated decahedral motif, *Phys. Rev. Lett.*, 1997, **79**, 1873.
19 M.-C. Daniel and D. Astruc, Gold nanoparticles: assembly, supramolecular chemistry, quantum-size-related properties, and applications toward biology, catalysis, and nanotechnology, *Chem. Rev.*, 2004, **104**, 293–346.
20 V. Novotny, P. Meincke and J. Watson, Effect of size and surface on the specific heat of small lead particles, *Phys. Rev. Lett.*, 1972, **28**, 901.
21 J. Dickey and A. Paskin, Phonon spectrum changes in small particles and their implications for superconductivity, *Phys. Rev. Lett.*, 1968, **21**, 1441.
22 R. Kubo, Electronic properties of metallic fine particles. I, *J. Phys. Soc. Jpn.*, 1962, **17**, 975–986.
23 A. Kawabata and R. Kubo, Electronic properties of fine metallic particles. II. Plasma resonance absorption, *J. Phys. Soc. Jpn.*, 1966, **21**, 1765–1772.
24 F. W. Halperin, Quantum size effects in metal particles, *Rev. Mod. Phys.*, 1986, **58**, 533.
25 C.-Y. Li, S. K. Karna, C.-W. Wang and W.-H. Li, Spin polarization and quantum spins in Au nanoparticles, *Int. J. Mol. Sci.*, 2013, **14**, 17618–17642.
26 H. Hori, T. Teranishi, Y. Nakae, Y. Seino, M. Miyake and S. Yamada, Anomalous magnetic polarization effect of Pd and Au nano-particles, *Phys. Lett. A*, 1999, **263**, 406–410.
27 Y. Yamamoto, T. Miura, M. Suzuki, N. Kawamura, H. Miyagawa, T. Nakamura, K. Kobayashi, T. Teranishi and H. Hori, Direct observation of ferromagnetic spin polarization in gold nanoparticles, *Phys. Rev. Lett.*, 2004, **93**, 116801.
28 J. S. Garitaonandia, M. Insausti, E. Goikolea, M. Suzuki, J. D. Cashion, N. Kawamura, H. Ohsawa, I. Gil de Muro, K. Suzuki, F. Plazaola, *et al.*, Chemically induced permanent magnetism in Au, Ag, and Cu nanoparticles: localization of themagnetism by element selective techniques, *Nano Lett.*, 2008, **8**, 661–667.
29 K. S. Krishna, P. Tarakeshwar, V. Mujica and C. S. Kumar, Chemically induced magnetism in atomically precise gold clusters, *Small*, 2014, **10**, 907–911.
30 M. Agrachev, S. Antonello, T. Dainese, M. Ruzzi, A. Zoleo, E. Aprá, N. Govind, A. Fortunelli, L. Sementa and F. Maran, Magnetic ordering in gold nanoclusters, *ACS Omega*, 2017, **2**, 2607–2617.
31 Y. Li and R. Jin, Magnetism of atomically precise gold and doped nanoclusters: delocalized spin and interparticle coupling, *J. Phys. Chem. C*, 2021, **125**, 15773–15784.
32 P. Zhang and T. Sham, Tuning the electronic behavior of Au nanoparticles with capping molecules, *Appl. Phys. Lett.*, 2002, **81**, 736–738.
33 P. Zhang and T. Sham, X-ray studies of the structure and electronic behavior of alkanethiolate-capped gold nanoparticles: the interplay of size and surface effects, *Phys. Rev. Lett.*, 2003, **90**, 245502.
34 J. Kübler, *Theory of itinerant electron magnetism*, Oxford University Press, 2017, pp. 106.
35 H. C. Siegmann and J. Stöhr, *Magnetism: From Fundamentals to Nanoscale Dynamics*, Springer Bln, 2006.
36 P. Crespo, R. Litrán, T. Rojas, M. Multigner, J. De la Fuente, J. Sánchez-López, M. García, A. Hernando, S. Penadés and A. Fernández, Permanent magnetism, magnetic anisotropy, and hysteresis of thiol-capped gold nanoparticles, *Phys. Rev. Lett.*, 2004, **93**, 087204.
37 A. Ayuela, P. Crespo, M. García, A. Hernando and P. M. Echenique, sp magnetism in clusters of gold thiolates, *New J. Phys.*, 2012, **14**, 013064.
38 M. Suzuki, N. Kawamura, H. Miyagawa, J. S. Garitaonandia, Y. Yamamoto and H. Hori, Measurement of a Pauli and orbital paramagnetic state in bulk gold using X-ray magnetic circular dichroism spectroscopy, *Phys. Rev. Lett.*, 2012, **108**, 047201.
39 V. Sahni and K.-P. Bohnen, Image charge at a metal surface, *Phys. Rev. B: Condens. Matter Mater. Phys.*, 1985, **31**, 7651.
40 M. K. Harbola and V. Sahni, Structure of the Fermi hole at surfaces, *Phys. Rev. B: Condens. Matter Mater. Phys.*, 1988, **37**, 745.
41 P. Dutta, S. Pal, M. Seehra, M. Anand and C. Roberts, Magnetism in dodecanethiol-capped gold nanoparticles: Role of size and capping agent, *Appl. Phys. Lett.*, 2007, **90**, 213102.
42 M. Hasan, D. Bethell and M. Brust, The fate of sulfur-bound hydrogen on formation of self-assembled thiol monolayers on gold: ^{1}H NMR spectroscopic evidence from solutions of gold clusters, *J. Am. Chem. Soc.*, 2002, **124**, 1132–1133.
43 R. G. Nuzzo, B. R. Zegarski and L. H. Dubois, Fundamental studies of the chemisorption of organosulfur compounds on gold (111). Implications for molecular self-assembly on gold surfaces, *J. Am. Chem. Soc.*, 1987, **109**, 733–740.
44 I. I. Rzeźnicka, J. Lee, P. Maksymovych and J. T. Yates, Nondissociative chemisorption of short chain alkanethiols on Au (111), *J. Phys. Chem. B*, 2005, **109**, 15992–15996.
45 H. Grönbeck, A. Curioni and W. Andreoni, Thiols and disulfides on the Au (111) surface: the headgroup- gold interaction, *J. Am. Chem. Soc.*, 2000, **122**, 3839–3842.
46 H. Guesmi, N. B. Luque, E. Santos and F. Tielens, Does the S- H Bond Always Break after Adsorption of an Alkylthiol on Au (111)?, *Chem. – Eur. J.*, 2017, **23**, 1402–1408.
47 M. S. Inkpen, Z.-F. Liu, H. Li, L. M. Campos, J. B. Neaton and L. Venkataraman, Non-chemisorbed gold–sulfur binding prevails in self-assembled monolayers, *Nat. Chem.*, 2019, **11**, 351–358.
48 M. Jaccob, G. Rajaraman and F. Totti, On the kinetics and thermodynamics of S–X (X = H, CH 3, SCH 3, COCH 3, and CN) cleavage in the formation of self-assembled monolayers of alkylthiols on Au (111), *Theor. Chem. Acc.*, 2012, **131**, 1–11.
49 G. Rajaraman, A. Caneschi, D. Gatteschi and F. Totti, A periodic mixed gaussians–plane waves DFT study on simple

thiols on Au (111): adsorbate species, surface reconstruction, and thiols functionalization, *Phys. Chem. Chem. Phys.*, 2011, **13**, 3886–3895.
50 H. Häkkinen, The gold–sulfur interface at the nanoscale, *Nat. Chem.*, 2012, **4**, 443–455.
51 L. Noodleman, Valence bond description of antiferromagnetic coupling in transition metal dimers, *J. Phys. Chem.*, 1981, **74**, 5737–5743.
52 L. Noodleman, D. A. Case and A. Aizman, Broken symmetry analysis of spin coupling in iron-sulfur clusters, *J. Am. Chem. Soc.*, 1988, **110**, 1001–1005.
53 K. Yamaguchi, Y. Takahara, T. Fueno and K. Nasu, Ab initio MO calculations of effective exchange integrals between transition-metal ions via oxygen dianions: nature of the copper-oxygen bonds and superconductivity, *Jpn. J. Appl. Phys.*, 1987, **26**, L1362.
54 A. D. Becke, Densityfunctional thermochemistry. III. the role of exact exchange, *J. Chem. Phys.*, 1993, **98**, 5648–5652.
55 F. Weigend and R. Ahlrichs, Balanced basis sets of split valence, triple zeta valence and quadruple zeta valence quality for H to Rn: Design and assessment of accuracy, *Phys. Chem. Chem. Phys.*, 2005, **7**, 3297–3305.
56 R. L. Martin and F. Illas, Antiferromagnetic exchange interactions from hybrid density functional theory, *Phys. Rev. Lett.*, 1997, **79**, 1539.
57 F. Bischoff, O. Hübner, W. Klopper, L. Schnelzer, B. Pilawa, M. Horvatić and C. Berthier, Density-functional calculation of the quadrupole splitting in the 23 Na NMR spectrum of the ferric wheel Na@ Fe 6 (tea) 6+ for various broken-symmetry states of the Heisenberg spin model, *Eur. Phys. J. B*, 2007, **55**, 229–235.
58 O. Hübner, K. Fink and W. Klopper, The spin coupling in the diiron complex [Fe2(hpdta)(H_2O)3Cl], *Phys. Chem. Chem. Phys.*, 2007, **9**, 1911–1920.
59 E. Ruiz, P. Alemany, S. Alvarez and J. Cano, Toward the prediction of magnetic coupling in molecular systems: hydroxo-and alkoxo-bridged Cu(II) binuclear complexes, *J. Am. Chem. Soc.*, 1997, **119**, 1297–1303.
60 H. Nieber, K. Doll and G. Zwicknagl, Ab initio correlation approach to a ferric wheel-like molecular cluster, *Eur. Phys. J. B*, 2006, **51**, 215–221.
61 M. Wojciechowski, B. Brzostowski and G. Kamieniarz, DFT Estimation of Exchange Coupling Constant of Cr_8 Molecular Ring using the Hybrid Functional B3LYP, *Acta Phys. Pol., A*, 2015, **127**, 407–409.
62 F. Neese, F. Wennmohs, A. Hansen and U. Becker, Efficient, approximate and parallel Hartree–Fock and hybrid DFT calculations. A 'chain-of-spheres' algorithm for the Hartree–Fock exchange, *Chem. Phys.*, 2009, **356**, 98–109.
63 M. Khatun, R. S. Majumdar and A. Anoop, A Global Optimizer for Nanoclusters, *Front. Chem.*, 2019, **7**, 644.
64 A. Deka and R. C. Deka, Structural and electronic properties of stable Aun (n = 2–13) clusters: A density functional study, *J. Mol. Struct.: THEOCHEM*, 2008, **870**, 83–93.
65 S. Bulusu and X. C. Zeng, Structures and relative stability of neutral gold clusters: Aun (n = 15–19), *J. Phys. Chem.*, 2006, **125**, 154303.
66 N. Jabr and A. Kodlaa, Dft study of small gold clusters aun (n = 2–13): The structural, electronic, thermodynamic and spectral properties, *Chem. Mater. Res.*, 2017, **9**, 17–27.
67 B. Zhu, D. Die, R.-C. Li, H. Lan, B.-X. Zheng and Z.-Q. Li, Insights into the structural, electronic and magnetic properties of Ni-doped gold clusters: Comparison with pure gold clusters, *J. Alloys Compd.*, 2017, **696**, 402–412.
68 P. V. Nhat, N. T. Si, J. Leszczynski and M. T. Nguyen, Another look at structure of gold clusters Au_n from perspective of phenomenological shell model, *Chem. Phys.*, 2017, **493**, 140–148.
69 B. R. Goldsmith, J. Florian, J.-X. Liu, P. Gruene, J. T. Lyon, D. M. Rayner, A. Fielicke, M. Scheffler and L. M. Ghiringhelli, Two-to-three dimensional transition in neutral gold clusters: The crucial role of van der Waals interactions and temperature, *Phys. Rev. Mater.*, 2019, **3**, 016002.
70 G. A. Bishea and M. D. Morse, Spectroscopic studies of jet-cooled AgAu and Au2, *J. Chem. Phys.*, 1991, **95**, 5646–5659.
71 K. C. Ko, D. Cho and J. Y. Lee, Systematic approach to design organic magnetic molecules: strongly coupled diradicals with ethylene coupler, *J. Phys. Chem. A*, 2012, **116**, 6837–6844.
72 I.-R. Jeon, J. G. Park, D. J. Xiao and T. D. Harris, An azophenine radical-bridged Fe2 single-molecule magnet with record magnetic exchange coupling, *J. Am. Chem. Soc.*, 2013, **135**, 16845–16848.
73 R. Khurana, A. Bajaj, K. Shamasundar and M. E. Ali, High-Spin Blatter's Triradicals, *J. Phys. Chem. A*, 2023, **127**, 7802–7810.
74 A. K. Pal, D. R. Mañeru, I. A. Latif, I. d. P. Moreira, F. Illas and S. N. Datta, Theoretical and computational investigation of meta-phenylene as ferromagnetic coupler in nitronyl nitroxide diradicals, *Theor. Chem. Acc.*, 2014, **133**, 1–12.
75 D. Bhattacharya, S. Shil, A. Misra and D. Klein, Intramolecular ferromagnetic coupling in bis-oxoverdazyl and bis-thioxoverdazyl diradicals with polyacene spacers, *Theor. Chem. Acc.*, 2010, **127**, 57–67.
76 S. Shil, D. Bhattacharya, A. Misra and L. Bytautas, Antiaromatic Molecules as Magnetic Couplers: A Computational Quest, *J. Phys. Chem. A*, 2024, **128**, 815–828.
77 C. Stroh, R. Ziessel, G. Raudaschl-Sieber, F. H. Köhler and P. Turek, Intramolecular exchange interactions in non-aromatic bis-nitronyl-nitroxides, *J. Mater. Chem.*, 2005, **15**, 850–858.
78 D. Cho, K. C. Ko and J. Y. Lee, Organic magnetic diradicals (radical–coupler–radical): standardization of couplers for strong ferromagnetism, *J. Phys. Chem. A*, 2014, **118**, 5112–5121.
79 M. E. Ali, A. S. Roy and S. N. Datta, Molecular tailoring and prediction of strongly ferromagnetically coupled trimethyl-

enemethane-based nitroxide diradicals, *J. Phys. Chem. A*, 2007, **111**, 5523–5527.

80 A. Bencini, D. Gatteschi, F. Totti, D. N. Sanz, J. A. Mc Cleverty and M. D. Ward, Density functional modeling of long range magnetic interactions in binuclear oxomolybdenum(v) complexes, *J. Phys. Chem. A*, 1998, **102**, 10545–10551.

81 M. Cui, Y. Zhao and Q. Song, Synthesis optical properties and applications of ultra-small luminescent gold nanoclusters, *TrAC, Trends Anal. Chem.*, 2014, **57**, 73–82.

82 J. Zheng, C. Zhang and R. M. Dickson, Highly fluorescent, water-soluble, size-tunable gold quantum dots, *Phys. Rev. Lett.*, 2004, **93**, 077402.

83 P. Dong, E. A. Fisher, M.-V. Meli and S. Trudel, Tuning the magnetism of gold nanoparticles by changing the thiol coating, *Nanoscale*, 2020, **12**, 19797–19803.

84 H. Zhang, K. Suzuki, K. Saito, J. Garitaonandia, E. Goikolea and M. Insausti, Effect of Organic Capping on the Magnetic Properties of Au Nanoparticles, *Mater. Sci. Forum*, 2010, **654**, 1174–1177.